

Organic compounds from macroalgal emission dominate new particle growth initiated by iodine species in coastal atmosphere

Yibei Wan¹, Xiangpeng Huang², Chong Xing¹, Qiongqiong Wang³, Xinlei Ge², and Huan Yu¹

¹China University of Geosciences

²Nanjing University of Information Science & Technology

³The Hong Kong University of Science and Technology

November 30, 2022

Abstract

Iodine-initiated new particle formation (I-NPF) has long been recognized in coastal hotspot regions. However, no prior work has studied the exact chemical composition of organic compounds and their role in the coastal I-NPF. Here we present an important complementary study to the ongoing laboratory and field researches of iodine nucleation in coastal atmosphere. Oxidation and NPF experiments with vapor emissions from real-world coastal macroalgae were simulated in a bag reactor. On the basis of comprehensive mass spectrometry measurements, we reported for the first time a series of volatile precursors and their oxidation products in gas and particle phases in such a highly complex system. Organic compounds overwhelmingly dominated over iodine in the new particle growth initiated by iodine species. This study provided a more complete story of coastal NPF from low-tide macroalgal emission.

Hosted file

si_gr1.docx available at <https://authorea.com/users/560450/articles/608457-organic-compounds-from-macroalgal-emission-dominate-new-particle-growth-initiated-by-iodine-species-in-coastal-atmosphere>

Organic compounds from macroalgal emission dominate new particle growth initiated by iodine species in coastal atmosphere

Yibei Wan¹, Xiangpeng Huang², Chong Xing¹, Qiongqiong Wang¹, Xinlei Ge², Huan Yu^{1,*}

¹ School of Environmental Studies, China University of Geosciences, Wuhan, 430074, China

² Jiangsu Key Laboratory of Atmospheric Environment Monitoring and Pollution Control, Collaborative Innovation Center of Atmospheric Environment and Equipment Technology, School of Environmental Science and Engineering, Nanjing University of Information Science and Technology, Nanjing 210044, China

* To whom correspondence should be addressed: yuhuan@cug.edu.cn

Abstract

Iodine-initiated new particle formation (I-NPF) has long been recognized in coastal hotspot regions. However, no prior work has studied the exact chemical composition of organic compounds and their role in the coastal I-NPF. Here we present an important complementary study to the ongoing laboratory and field researches of iodine nucleation in coastal atmosphere. Oxidation and NPF experiments with vapor emissions from real-world coastal macroalgae were simulated in a bag reactor. On the basis of comprehensive mass spectrometry measurements, we reported for the first time a series of volatile precursors and their oxidation products in gas and particle phases in such a highly complex system. Organic compounds overwhelmingly dominated over iodine in the new particle growth initiated by iodine species. This study provided a more complete story of coastal NPF from low-tide macroalgal emission.

1. Introduction

Coastal new particle formation (NPF) may be driven by daytime low-tide emission of iodine species from macroalgae fully or partially exposed to the air. The phenomenon was reported in hotspot locations of west Europe, Australia and polar regions [Allan *et al.*, 2015; Baccarini *et al.*, 2020; Beck *et al.*, 2021; Heard *et al.*, 2006; McFiggans *et al.*, 2010; O'Dowd *et al.*, 2002; Sipilä *et al.*, 2016; Whitehead *et al.*, 2009]. In the southeast coastline of China, we reported intense iodine-initiated NPF based on particle number size distribution and iodine measurements [Yu *et al.*, 2019].

To simulate iodine-initiated NPF (I-NPF) in controlled laboratory conditions, I₂ or CH₂I₂ vapor

was usually photolyzed in the presence of ozone to provide nucleation precursor [Burkholder et al., 2004; He et al., 2021; Huang et al., 2022; Jimenez et al., 2003; Martín et al., 2020; Monahan et al., 2012; O'Dowd et al., 2004; Saunders and Plane, 2005]. Ashu-Ayem et al. [2012]; McFiggans et al. [2004]; Monahan et al. [2012]; Sellegri et al. [2005] and Sellegri et al. [2016] also investigated the NPF from the vapors emitted by real-world macroalgal specimens or seawater in laboratory chamber or apparatus. However, the focus of all above studies are emission rate, oxidation mechanisms or nucleation pathways of iodine species. For example, positive correlations between particle concentrations and I_2 or CH_2I_2 mixing ratios were usually observed [Burkholder et al., 2004; Jimenez et al., 2003; Monahan et al., 2012; Sellegri et al., 2005]. Kinetic studies in flow tube or CERN CLOUD chamber proposed the clustering of iodine oxides (I_xO_y) or iodine oxoacids (HIO_3 , HIO_2) as nucleation mechanisms on the basis of photoionization TOF-MS [Martín et al., 2020], Api-TOF and nitrate-Chemical Ionization Mass Spectrometer (CIMS) measurements [He et al., 2021]. A recent chamber study showed heterogeneous reaction between iodine oxide nanoparticle, meso-erythritol (or glyoxal) and dimethylamine accelerated nanoparticle growth [Huang et al., 2022].

Until now, no prior work has investigated the exact chemical identity of organic compounds (other than iodinated methane) and their role in I-NPF. The role of biogenic terpenes and anthropogenic aromatics in continental NPF has been recognized for a long time [Donahue et al., 2013]. Their ozonolysis or photochemistry products have been investigated in depth by using Electrospray Ionization Mass Spectrometry (ESI-MS) and more recently CIMS [Ehn et al., 2014; Faxon et al., 2018; Kundu et al., 2012; Kundu et al., 2017; Nguyen et al., 2010; Riva et al., 2017; Wang et al., 2020; Yan et al., 2020]. It is very likely that certain volatile organic compounds (VOCs) emitted mutually with iodine or iodinated methane from coastal biota or biologically active sea surface may also be involved in coastal I-NPF process and promote the growth of iodine particles.

To test this hypothesis, we conducted oxidation and NPF experiments with vapor emissions from real-world coastal macroalgae in a bag reactor. A suite of mass spectrometric methods including Inductively Coupled Plasma-MS (ICP-MS), Gas Chromatography-MS (GC-MS), ESI-orbitrap MS and iodide-CIMS were applied to measure vapor precursors, gaseous products and particulate products during the NPF process. Mass concentrations of total organic carbon (TOC) and total iodine (TI) of new particles were compared to evaluate the relative importance of organics and iodine in new particle growth. The identity and transformation mechanisms of organic compounds were identified to provide a more complete story of coastal NPF from low-tide macroalgal emission. Our study is thus complementary to prior laboratory and field studies of I-NPF, but has an emphasis on organics.

2. Experiments

2.1 Experimental apparatus and sample collection

Similar to Potential Aerosol Mass (PAM) Oxidation Flow Reactor, a bag reactor was designed to provide an oxidizing environment for simulating atmospheric oxidation processes of algae-emitted VOCs. The bag reactor was made from 75 μm -thick fluorinated ethylene propylene (FEP) Teflon (1.2 m \times 1.5 m, flat dimension). The volume of the bag at full inflation was determined experimentally to be about 200 L. The bag was suspended vertically (Figure S1) and kept in the dark or directly exposed to room light of fluorescent lamp. Because the purpose of this study is to qualitatively measure the oxidation products of algae-emitted VOCs, wall loss, production rate and other kinetic factors in the bag reactor were not evaluated. Fresh macroalgae (*Undaria pinnatifida*) was collected from intertidal zone at Xiangshan gulf of east China coast and stored at -10 °C until the experiments. 2 kg macroalgae was put in a 20 L Pyrex glass bottle that was filled with ~1 L natural seawater. The specimens was partially exposed to the air to simulate tidal emersion of macroalgae. A flow of particle-free ultra high purity (UHP) air blew the algae-emitted VOCs out of the bottle and merged with a diluting air flow before entering the bag reactor.

Two types of experiments were conducted. In the three ozonolysis experiments, ozone (O_3) was generated by flowing an UHP air flow through a 5 Watts 185 nm UV lamp. The O_3 flow was fed just before the bag reactor was fully inflated. Final O_3 concentration in the bag reactor was measured to be ~200 ppbv using an ozone analyzer (Model 49i, Thermo-Fisher Scientific Inc.). In an additional OH-enhanced experiment, the O_3 /VOC mixture flow was directed through a 254 nm UV light before entering the bag reactor. OH radicals were produced via the reaction $\text{O}_3+h\nu\rightarrow\text{O}_2+\text{O}(^1\text{D})$ and $\text{O}(^1\text{D})+\text{H}_2\text{O}\rightarrow 2\text{OH}$.

Before each experiment, the bag was purged for several hours to reduce background particle concentrations to below 1 cm^{-3} . The bag reactor was first operated in a static mode to monitor the time evolution of gaseous products and particle size, and then in a dynamic mode to collect enough particles for offline chemical analysis. In the static mode, the bag was first filled to full inflation with the VOCs/ O_3 flows. The flows were then shut down; a Scanning Mobility Particle Sizer (SMPS, model 3936, TSI Inc., Shoreview, MN, USA) and an Aerodyne iodide-CIMS pulled two flows of 0.3 liters per minute (lpm) and 1.8 lpm out of the bag, respectively. The SMPS measured the particle number size distribution from 14 to 600 nm.

In the dynamic mode, the VOCs/ O_3 flow of 3 lpm was fed to the bag continuously, while the

SMPS and a vacuum pump (GAST Group Ltd.) pulled sample flows of 0.3 and 2.7 lpm, respectively, out of the bag reactor. This resulted in an overall residential time of 67 minutes for the O₃/VOC mixture in the fully inflated bag. The particles in the 2.7 lpm sample flow were collected onto a Zefluor® PTFE membrane filter mounted in a filter inlet for gases and aerosols (FIGAERO) for iodide-CIMS analysis, or alternatively, onto 47 mm diameter double quartz fiber filter pack mounted in a filter holder for ESI-orbitrap MS, ICP-MS and TOC analysis. The front filter of the double filter pack collected the particles, while the back filter placed downstream of the front filter was supposed to adsorb the same amount of volatile species as the front filter.

2.2 Chemical analysis

Before the ozonolysis experiments, the algae-emitted VOCs in the bag reactor was collected by a 6-liter pre-evacuated stainless-steel canisters (Entech Instruments, Inc., Simi Valley, CA, USA) and was analyzed using a quadrupole GC-MS system (model TH-300B, Wuhan Tianhong Instruments Co. Ltd., Wuhan, China). The algae-emitted VOCs, as well as their gaseous and particulate products, were also measured by the FIGAERO-iodide-CIMS. Iodide-adduct chemical ionization is well suited for measuring oxygenated or acidic compounds with minimal fragmentation. More details of the GC-MS and FIGAERO-iodide-CIMS measurements can be found in Supporting Material. The theory and design of the two instruments were described by *Wang et al. [2014]* and *Lopez-Hilfiker et al. [2014]*.

The particles collected on quartz fiber filters were sent for offline quantification of TOC and TI, as well as non-target analysis of organic compounds using ESI-orbitrap MS. The front and back filters were treated, separately, following the procedure as below: the filter was ultrasonicated twice with 10-mL water and acetone nitrile solvent mixture (v:v=1:1). The extract was filtered by a 0.2 µm PTFE syringe filter and evaporated in a rotary evaporator to 0.5 mL. After being centrifuged for 30 min at 12000 rpm, the supernatant was collected for TI analysis by Agilent 1100 HPLC-7900 ICP-MS (Agilent Technologies, Santa Clara, CA, USA) and TOC analysis by a TOC analyzer (Model TOC-5000A, Shimadzu, Japan). TI or TOC in the particles was obtained by subtracting the amount on the back filter from that on the front filter. Nontarget analysis of organic compounds in the supernatant was conducted using a Q Exactive hybrid Quadrupole-Orbitrap mass spectrometer (Thermo Scientific, Bremen, Germany). The supernatant was directly infused by a syringe pump and ionized in negative ESI source. All the ions in the m/z range from 50 to 500 Th were scanned with a mass resolution of 70000. The chemically sound CHO molecular formulas were computed with a mass tolerance of ±2 ppm for these ions. Only the compounds that existed solely in the front filter or

with ion intensity in the front filter higher than that in the back filter by a factor of 3 were regarded as the organic compounds in the particle phase.

3. Results and discussion

3.1 Relative mass contribution of organic carbon and iodine to new particles

Typical banana-shape particle size spectrum observed in the static mode of an ozonolysis experiment is shown in Figure 1a. In the presence of room light, new particles larger than 14 nm were observed only 58 minutes after the injection of ozone flow. This relative long time is due to the build-up of O₃ concentration and subsequent accumulation of oxidation products. No particles were formed in the absence of room light or ozone. In the dynamic mode experiments, O₃ in the bag reactor was kept at its maximum concentration 200 ppbv. With a prolonged residential time of 67 min, the particles grew to 102±23 nm, which was measured by the SMPS at the outlet of the bag reactor. The TOC and TI measurements show that organic compounds contributed more particle mass than iodine with TOC/(I+TOC) ratio of 96.1±2.9% (Table 1).

In the OH-enhanced experiment (dynamic mode), more particulate products were generated with enhanced oxidation capacity: TI in the particles increased by a factor of 10.8; TOC increased by a factor of 2.7; particle number concentration increased by a factor of 7.4. On the other hand, particle size decreased to 73 nm and TOC/(TI+TOC) ratio decreased to 92.9% (Table 1). These differences indicate that more iodine nuclei were produced with enhanced OH concentration, probably via $\text{OIO} + \text{OH} \rightarrow \text{HOIO}_2$ [Plane et al., 2006]. Competitive uptake of condensing organic vapors onto these iodine nuclei limited the growth of individual new particles. Nevertheless, organic compounds overwhelmingly dominated over iodine in the mass contribution to new particle growth.

The significant organic contribution observed in the laboratory condition is generally consistent with TOC/(I+TOC) ratio of 98.2% in 10-56 nm new particles collected during a coastal I-NPF event in China [Yu et al., 2019], although TOC and TI during the field event are two orders of magnitude lower than those in the bag reactor (Table 1). Mean diameter of new particles was observed to be only 16 nm during the field event. But those small new particles are expected to grow into CCN active sizes, given longer residence time and uptake of more condensing vapors in the atmosphere.

3.2 Macroalgal emission

It is of particular interest to know what VOCs are emitted from coastal macroalgae. They are potential precursors of iodine particle nucleation and growth. The canister sampling followed by

GC-MS analysis showed that the top 9 non-CHO compounds with highest TIC peak areas (Table 2) are C₅ alkanes, C₁₀ alpha-pinene and halogenated C₁, C₃ and C₅ alkanes. The top 10 CHO compounds are C₂-C₆ alcohols and carbonyls with saturated or unsaturated carbon chain.

Iodide-CIMS is more sensitive to more oxygenated or acidic compounds and thus complementary to the GC-MS measurement. The 76 organic precursors detected by iodide-CIMS before ozone addition were characterized by C_{1,2,3,6} and O₂₋₃ formulas (Figure 2a). The top 7 compounds with highest ion intensities were CH₂O₂, C₂H₄O₂, C₃H₆O₃, C₆H₁₀O₃, C₂H₆O₂, C₄H₈O₂ and C₆H₁₂O₃, which accounted for 82.5% of total ion intensity. They are C₁-C₆ mono-carboxylic acids, hydroxyl carboxylic acids or oxo-carboxylic acids with 2 to 3 oxygen atoms (Table 2). Their carbon atom numbers are in general consistent with the VOCs detected by GC-MS.

Relatively high signals of HNO₃ were observed as NO₃⁻ and HNO₃I⁻ before the addition of ozone to the bag reactor. Because HNO₃ and HNO₂ were also observed as deprotonated ions or I⁻ clusters in the particle phase during the NPF, HNO₃ is also an important precursor of particle formation.

3.3 Gaseous and particulate products

3.3.1 Inorganic molecules and radicals

Being different from nitrate-CIMS, our iodide-CIMS did not detect nucleating clusters of iodine oxides or oxyacids after the addition of ozone. Instead, dozens of new inorganic molecules or radicals were observed as clusters with I⁻, NO₃⁻ or deprotonated ions in the gas or particle phase (Figure S2). We grouped these species by elemental composition and investigated their role in the NPF by observing how their gaseous ion intensities evolved during the NPF event in the bag reactor (Figure 1b-1e).

1. Cl, I, Cl₂ and ClI in the gas phase: the intensities of I and Cl increased ca. 10 minutes before 14 nm particles appeared and decreased as the particles grew up. Based on prior work of *Burkholder et al.* [2004]; *Jimenez et al.* [2003]; *O'Dowd et al.* [2004], we suggested the photolysis of CH₂Cl₂, CHBrCl, CH₃I and C₃H₇I was the source of halogen atoms (e.g., CH₃I+hν→CH₃+I). There was a time lag of 20-25 minutes between the appearances of Cl and I and those of ClI and Cl₂, which were probably from the recombination of Cl and I atoms.

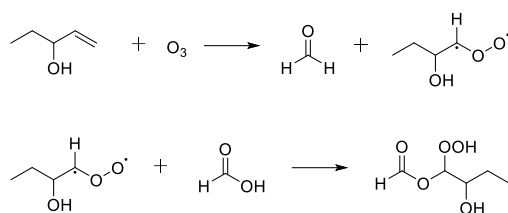
2. IO₂, IO, ClIO, INO₂ and ClNO₂ in the gas phase: these species showed a similar time series to I and Cl atoms. IO, IO₂ and ClIO could be from the reactions between I, ClI and O₃. INO₂ is usually thought to form upon the reaction I+NO₂+M→INO₂+M [Saiz-Lopez et al., 2012]. ClNO₂ was likely to form upon similar reaction between Cl and NO₂ in the bag reactor.

3. HIO₃ and INO₃: the two species seem to be the end products of above intermediates, because their intensities kept on increasing during new particle growth. INO₃, which is iodine nitrate IONO₂, was detected in both gas and particle phases. IONO₂ probably formed upon the recombination of IO and NO₂ (IO+NO₂+M→IONO₂+M) [Saiz-Lopez *et al.*, 2012]. HIO₃ was likely to form via OIO+OH→HOIO₂ or I + H₂O + O₃→HOIO₂ + OH [Martín *et al.*, 2020; Plane *et al.*, 2006]. HIO₃ was not detected in particle phase by iodide-CIMS, which is contrary to the observation by HPLC-ICP-MS that total iodine was mostly dominated IO₃⁻ peak. The signals of IO⁻, IO₂⁻ and HIONO₃⁻ in the particle phase are therefore most likely to result from thermal decomposition of HIO₃ to HIO and HIO₂ in the FIGAERO thermal desorption process.

4. CH₃SO₃H, S₂⁻, S₃⁻, SO₃⁻: We observed methane sulfonic acid (CH₃SO₃H, MSA) in both gas and particle phases. Gaseous MSA increased in the beginning, but decreased after new particles appeared (Figure 1f). Apparently, our measurement suggested MSA contributed to the growth of new particles, but it is unknown if it also participated in nucleation. We suggested S₂⁻, S₃⁻, SO₃⁻ ions observed in the particle phase were thermal decomposition products of MSA.

3.3.2 Gaseous organic products

After ozone addition, a gradual transformation from C₁-C₃ precursors to C₅-C₈ gaseous products was observed during the NPF process (Figure 1h). In the meanwhile, the oxygen atom number of the compounds increased from 2-3 to 4-7 (Figure 1g). The formation of compounds with more carbon atoms than the parent VOCs is unlikely in the gas phase, except bimolecular reactions of stabilized Criegee intermediates (SCIs) that typically form upon alkene ozonolysis. Similar to isoprene ozonolysis [Inomata *et al.*, 2014; Riva *et al.*, 2017], we propose the SCI addition mechanism can also explain the transformation observed in our case: (1) C₄ SCIs formed upon the ozonolysis of CHO precursors with C=C double bonds (e.g., those observed by GC-MS in Table 2). (2) the insertion of C₄ SCIs into carboxylic acid precursors (e.g., those observed by CIMS in Table 2) produced oligomeric hydroperoxides. An example was shown in Scheme I for the reactions of most abundant ethyl vinyl carbinol (C₅H₁₀O), ozone and formic acid (CH₂O₂), but the same mechanism is also applicable for ethyl vinyl ketone (C₅H₈O) and other abundant C₂-C₅ carboxylic acids and hydroxyl carboxylic acids. As a result, a series of gaseous oligomeric hydroperoxides C₅H₁₀O₅, C₆H₁₀O₅, C₆H₁₂O₅, C₇H₁₂O₆, C₇H₁₄O₆, C₈H₁₄O₅, C₈H₁₆O₆, C₈H₁₆O₅ and C₉H₁₆O₆ were observed with high intensity by iodide-CIMS.



Scheme I

3.3.3 Particulate organic products

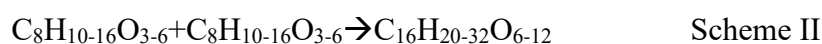
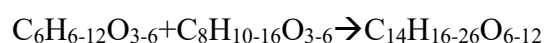
In the end of a typical ozonolysis experiment (dynamic mode), 100 and 364 new formulas were observed in the gas and particle phases, respectively, including 73 semi-VOCs appeared in both gas and particle phases. Those semi-VOCs accounted for 81 and 20% of total ion intensities of gaseous and particulate products, respectively. Being different from unimodal atom number distributions of gaseous products ($C_{\max}=7$ and $O_{\max}=5$, Figure 2b), particulate products were characterized by distinct bimodal or trimodal distribution of carbon number ($C_{\max}=8, 14$ and 16 , Figure 2c) and oxygen number ($O_{\max}=4$ and 8), implying possible dimer formation via accretion reactions in the particle phase.

ESI-Orbitrap MS differs from FIGAERO-iodide-CIMS in extraction method (ultrasonic solvent extraction from quartz fiber filter *vs.* thermal desorption from PTFE membrane filter), ionization source (electrospray ionization *vs.* iodide-adduct chemical ionization) and MS resolving power (70000 *vs.* 4500). The result showed that ESI-orbitrap MS and FIGAERO-iodide-CIMS detected 336 and 364 organic formulas, respectively, in the particle phase. 167 organic formulas were commonly observed by both methods, which accounted for 87% and 54% of total ion intensity of organic formulas by the two methods, respectively (Figure S3). As shown in Figure 2c and 2d, FIGAERO-iodide-CIMS had better sensitivity toward the organic compounds with more oxygen atoms (e.g., $O \geq 8$) and carbon atoms (e.g., $C \geq 10$). As a result, bimodal carbon and oxygen atom number distributions were observed by FIGAERO-iodide-CIMS, but not ESI-orbitrap MS.

The measurement by ESI-orbitrap MS provided more insights about the formation mechanism of particulate products. We compared the 336 formulas detected by ESI-orbitrap MS in our study with the 414 formulas of isoprene ozonolysis SOA products [Nguyen *et al.*, 2010] and 922 formulas of alpha-pinene ozonolysis SOA products [Putman *et al.*, 2012] measured by the ESI-orbitrap MS. It was found that 72% of the formulas in this study can also be found in isoprene SOA, but only 39% can be found in alpha-pinene SOA. This seems to imply that some similar alkene ozonolysis reactions occurred in our system and isoprene ozonolysis.

For such a highly complex system full of various algae-emitted precursors, it is impossible to

simply propose a reaction mechanism to explain the formation of all particulate products, nor to list all reactions occurring in the bag reactor. On the basis of particle-phase oligomer chemistry [Seinfeld and Pandis, 2016], especially the well-understood isoprene ozonolysis SOA chemistry [Inomata et al., 2014; Nguyen et al., 2010; Riva et al., 2017], we suggest a variety of accretion reactions without uniform oligomerization pattern (e.g., esterification, aldol condensation, hemiacetal reactions, peroxyhemiacetal formation and SCI reactions, etc.) transformed $O_{\max}=4$ and $C_{\max}=8$ multifunctional monomers (like alcohols, carbonyls, hydroperoxides, carboxylic acids) to $O_{\max}=8$ and $C_{\max}=14$ or 16 dimers. Scheme II illustrated addition type self- and cross-oligomerization between C_6 and C_8 monomers produces C_{14} and C_{16} dimers. All the formulas in Scheme II are among the most abundant ones observed in the particle phase by the iodide-CIMS.



4. Conclusions

Using a suite of mass spectrometers, we reported, for the first time, the chemical compositions of volatile precursors emitted by real-world coastal macroalgae and their gaseous and particulate oxidation products. In the presence of room light and ozone, the photolysis of halogenated $C_{1,3,5}$ alkanes ends up as HIO_3 and INO_3 . It was most likely HIO_3 initiated NPF and provided nuclei for the further condensation of other products like INO_3 , MSA and CHO compounds. Gas-phase SCI reactions and particle-phase accretion reactions transformed C_1 - C_6 and O_2 - O_3 precursors gradually to particulate products with $C_{\max}=8, 14$ and 16 and $O_{\max}=4$ and 8. As a result, organic carbon were found to overwhelmingly dominated over iodine in the mass contribution to the new particle growth. Although our instruments did not allow the detection of nucleating clusters of iodine oxides or oxyacids, our study provided important complementary information to the ongoing laboratory and field researches of coastal I-NPF.

Data Availability Statement

All data related to figures and tables in this study are archived and made available through Zenodo data repository <https://doi.org/10.5281/zenodo.6965859>.

Acknowledgement

This work was supported by the National Science Foundation of China (grant no. 41975831 and 42175131) and Start-up research funding from China University of Geosciences.

- Allan, J. D., et al. (2015), Iodine observed in new particle formation events in the Arctic atmosphere during ACCACIA, *Atmos. Chem. Phys.*, 15(10), 5599-5609, doi:10.5194/acp-15-5599-2015.
- Ashu-Ayem, E. R., U. Nitschke, C. Monahan, J. Chen, S. B. Darby, P. D. Smith, C. D. O'Dowd, D. B. Stengel, and D. S. Venables (2012), Coastal Iodine Emissions. 1. Release of I₂ by *Laminaria digitata* in Chamber Experiments, *Environmental Science & Technology*, 46(19), 10413-10421, doi:10.1021/es204534v.
- Baccarini, A., et al. (2020), Frequent new particle formation over the high Arctic pack ice by enhanced iodine emissions, *Nature Communications*, 11(1), 4924, doi:10.1038/s41467-020-18551-0.
- Beck, L. J., et al. (2021), Differing Mechanisms of New Particle Formation at Two Arctic Sites, *Geophysical Research Letters*, 48(4), e2020GL091334, doi:<https://doi.org/10.1029/2020GL091334>.
- Burkholder, J. B., J. Curtius, A. R. Ravishankara, and E. R. Lovejoy (2004), Laboratory studies of the homogeneous nucleation of iodine oxides, *Atmospheric Chemistry and Physics*, 4(1), 19-34, doi:10.5194/acp-4-19-2004.
- Donahue, N. M., et al. (2013), How do organic vapors contribute to new-particle formation?, *Faraday Discussions*, 165(0), 91-104, doi:10.1039/C3FD00046J.
- Ehn, M., et al. (2014), A large source of low-volatility secondary organic aerosol, *Nature*, 506(7489), 476-479, doi:10.1038/nature13032.
- Faxon, C., J. Hammes, M. Le Breton, R. K. Pathak, and M. Hallquist (2018), Characterization of organic nitrate constituents of secondary organic aerosol (SOA) from nitrate-radical-initiated oxidation of limonene using high-resolution chemical ionization mass spectrometry, *Atmospheric Chemistry and Physics*, 18(8), 5467-5481, doi:10.5194/acp-18-5467-2018.
- He, X. C., et al. (2021), Role of iodine oxoacids in atmospheric aerosol nucleation, *Science*, 371(6529), 589-595, doi:10.1126/science.abe0298.
- Heard, D. E., et al. (2006), The North Atlantic Marine Boundary Layer Experiment(NAMBLEX). Overview of the campaign held at Mace Head, Ireland, in summer 2002, *Atmos. Chem. Phys.*, 6(8), 2241-2272, doi:10.5194/acp-6-2241-2006.
- Huang, R.-J., et al. (2022), Heterogeneous iodine-organic chemistry fast-tracks marine new particle formation, *Proceedings of the National Academy of Sciences*, 119(32), e2201729119, doi:10.1073/pnas.2201729119.
- Inomata, S., K. Sato, J. Hirokawa, Y. Sakamoto, H. Tanimoto, M. Okumura, S. Tohno, and T. Imamura (2014), Analysis of secondary organic aerosols from ozonolysis of isoprene by proton transfer reaction mass spectrometry, *Atmospheric Environment*, 97, 397-405, doi:<https://doi.org/10.1016/j.atmosenv.2014.03.045>.
- Jimenez, J. L., R. Bahreini, D. R. Cocker III, H. Zhuang, V. Varutbangkul, R. C. Flagan, J. H. Seinfeld, C. D. O'Dowd, and T. Hoffmann (2003), New particle formation from photooxidation of diiodomethane (CH₂I₂), *Journal of Geophysical Research: Atmospheres*, 108(D10), doi:<https://doi.org/10.1029/2002JD002452>.
- Kundu, S., R. Fisseha, A. L. Putman, T. A. Rahn, and L. R. Mazzoleni (2012), High molecular weight SOA formation during limonene ozonolysis: insights from ultrahigh-resolution FT-ICR mass spectrometry characterization, *Atmos. Chem. Phys.*, 12(12), 5523-5536, doi:10.5194/acp-12-5523-2012.
- Kundu, S., R. Fisseha, A. L. Putman, T. A. Rahn, and L. R. Mazzoleni (2017), Molecular formula composition of β -caryophyllene ozonolysis SOA formed in humid and dry conditions, *Atmospheric Environment*, 154, 70-81, doi:<https://doi.org/10.1016/j.atmosenv.2016.12.031>.
- Lopez-Hilfiker, F. D., et al. (2014), A novel method for online analysis of gas and particle composition: description and evaluation of a Filter Inlet for Gases and AEROSols (FIGAERO),

326 *Atmospheric Measurement Techniques*, 7(4), 983-1001, doi:10.5194/amt-7-983-2014.

327 Martín, J. C. G., T. R. Lewis, M. A. Blitz, J. M. C. Plane, M. Kumar, J. S. Francisco, and A.

328 Saiz-Lopez (2020), A gas-to-particle conversion mechanism helps to explain atmospheric particle

329 formation through clustering of iodine oxides, *Nature Communications*, 11(1), 4521,

330 doi:10.1038/s41467-020-18252-8.

331 McFiggans, G., et al. (2010), Iodine-mediated coastal particle formation: an overview of the Reactive

332 Halogens in the Marine Boundary Layer (RHaMBLe) Roscoff coastal study, *Atmospheric*

333 *Chemistry and Physics*, 10(6), 2975-2999, doi:10.5194/acp-10-2975-2010.

334 McFiggans, G., et al. (2004), Direct evidence for coastal iodine particles from Laminaria macroalgae

335 – linkage to emissions of molecular iodine, *Atmos. Chem. Phys.*, 4(3), 701-713,

336 doi:10.5194/acp-4-701-2004.

337 Monahan, C., E. R. Ashu-Ayem, U. Nitschke, S. B. Darby, P. D. Smith, D. B. Stengel, D. S. Venables,

338 and C. D. O'Dowd (2012), Coastal Iodine Emissions: Part 2. Chamber Experiments of Particle

339 Formation from Laminaria digitata-Derived and Laboratory-Generated I₂, *Environmental Science*

340 *& Technology*, 46(19), 10422-10428, doi:10.1021/es3011805.

341 Nguyen, T. B., A. P. Bateman, D. L. Bones, S. A. Nizkorodov, J. Laskin, and A. Laskin (2010),

342 High-resolution mass spectrometry analysis of secondary organic aerosol generated by ozonolysis

343 of isoprene, *Atmospheric Environment*, 44(8), 1032-1042,

344 doi:<https://doi.org/10.1016/j.atmosenv.2009.12.019>.

345 O'Dowd, C. D., J. L. Jimenez, R. Bahreini, R. C. Flagan, J. H. Seinfeld, K. Hämeri, L. Pirjola, M.

346 Kulmala, S. G. Jennings, and T. Hoffmann (2002), Marine aerosol formation from biogenic iodine

347 emissions, *Nature*, 417, 632, doi:10.1038/nature00775.

348 O'Dowd, C. D., M. C. Facchini, F. Cavalli, D. Cebrunis, M. Mircea, S. Decesari, S. Fuzzi, Y. J. Yoon,

349 and J.-P. Putard (2004), Biogenically driven organic contribution to marine aerosol, *Nature*, 431,

350 676-680.

351 Plane, J. M. C., D. M. Joseph, B. J. Allan, S. H. Ashworth, and J. S. Francisco (2006), An

352 Experimental and Theoretical Study of the Reactions OIO + NO and OIO + OH, *The Journal of*

353 *Physical Chemistry A*, 110(1), 93-100, doi:10.1021/jp055364y.

354 Putman, A. L., J. H. Offenberg, R. Fisseha, S. Kundu, T. A. Rahn, and L. R. Mazzoleni (2012),

355 Ultrahigh-resolution FT-ICR mass spectrometry characterization of α -pinene ozonolysis SOA,

356 *Atmospheric Environment*, 46, 164-172, doi:<https://doi.org/10.1016/j.atmosenv.2011.10.003>.

357 Riva, M., S. H. Budisulistiorini, Z. F. Zhang, A. Gold, J. A. Thornton, B. J. Turpin, and J. D. Surratt

358 (2017), Multiphase reactivity of gaseous hydroperoxide oligomers produced from isoprene

359 ozonolysis in the presence of acidified aerosols, *Atmospheric Environment*, 152, 314-322,

360 doi:10.1016/j.atmosenv.2016.12.040.

361 Saiz-Lopez, A., J. M. C. Plane, A. R. Baker, L. J. Carpenter, R. von Glasow, J. C. Gómez Martín, G.

362 McFiggans, and R. W. Saunders (2012), Atmospheric Chemistry of Iodine, *Chemical Reviews*,

363 112(3), 1773-1804, doi:10.1021/cr200029u.

364 Saunders, R. W., and J. M. C. Plane (2005), Formation Pathways and Composition of Iodine Oxide

365 Ultra-Fine Particles, *Environmental Chemistry*, 2(4), 299-303,

366 doi:<https://doi.org/10.1071/EN05079>.

367 Seinfeld, J. H., and S. N. Pandis (2016), *Atmospheric chemistry and physics: from air pollution to*

368 *climate change*, 3rd ed., John Wiley and Sons. Inc., New York.

369 Sellegri, K., et al. (2016), Evidence of atmospheric nanoparticle formation from emissions of marine

370 microorganisms, *Geophysical Research Letters*, 43(12), 6596-6603,

371 doi:<https://doi.org/10.1002/2016GL069389>.

372 Sellegri, K., Y. J. Yoon, S. G. Jennings, C. D. O'Dowd, L. Pirjola, S. Cautenet, H. Chen, and T.

373 Hoffmann (2005), Quantification of Coastal New Ultra-Fine Particles Formation from In situ and

374 Chamber Measurements during the BIOFLUX Campaign, *Environmental Chemistry*, 2(4),

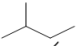

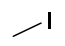
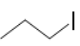
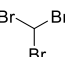
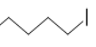
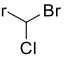
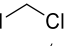
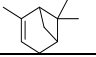
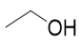
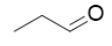
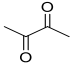
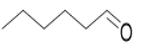
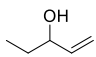
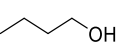
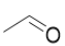
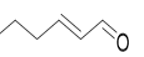
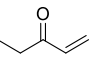
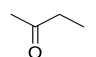
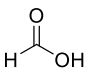
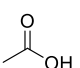
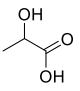
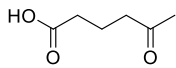
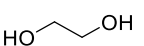
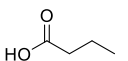
375 260-270, doi:<https://doi.org/10.1071/EN05074>.

- Sipilä, M., et al. (2016), Molecular-scale evidence of aerosol particle formation via sequential addition of HIO₃, *Nature*, *advance online publication*, doi:10.1038/nature19314
<http://www.nature.com/nature/journal/vaop/ncurrent/abs/nature19314.html#supplementary-information>.
- Wang, M., et al. (2020), Photo-oxidation of Aromatic Hydrocarbons Produces Low-Volatility Organic Compounds, *Environmental science & technology*, 54(13), 7911-7921, doi:10.1021/acs.est.0c02100.
- Wang, M., et al. (2014), Development and validation of a cryogen-free automatic gas chromatograph system (GC-MS/FID) for online measurements of volatile organic compounds, *Analytical Methods*, 6(23), 9424-9434, doi:10.1039/C4AY01855A.
- Whitehead, J. D., G. B. McFiggans, M. W. Gallagher, and M. J. Flynn (2009), Direct linkage between tidally driven coastal ozone deposition fluxes, particle emission fluxes, and subsequent CCN formation, *Geophysical Research Letters*, 36(4), doi:doi:10.1029/2008GL035969.
- Yan, C., et al. (2020), Size-dependent influence of NO(x) on the growth rates of organic aerosol particles, *Science advances*, 6(22), eaay4945, doi:10.1126/sciadv.aay4945.
- Yu, H., L. Ren, X. Huang, M. Xie, J. He, and H. Xiao (2019), Iodine speciation and size distribution in ambient aerosols at a coastal new particle formation hotspot in China, *Atmospheric Chemistry and Physics*, 19(6), 4025-4039, doi:10.5194/acp-19-4025-2019.

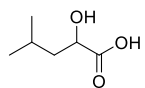
Table 1. Particle number concentration (N), mean diameter (D_p), total organic carbon (TOC) and total iodine (TI) of new particles with a residential time of 67 min in the bag reactor in the ozonolysis experiments and OH-enhanced experiment (dynamic mode). Those of 10-56 nm new particles collected by a nano Micro-Orifice Uniform Deposit Impactor (nano-MOUDI, MSP, Inc.) during an I-NPF event at a coastal site of Ningbo, China (Yu *et al.*, 2019) were also listed.

	TOC ($\mu\text{g m}^{-3}$)	TI ($\mu\text{g m}^{-3}$)	TOC/(TI+TOC)	N (cm^{-3})	D_p (nm)
ozonolysis experiments	45.6 \pm 9.7	0.88 \pm 0.34	96.1 \pm 2.9%	(5.58 \pm 2.04) $\times 10^4$	102 \pm 23
OH-enhanced experiment	125.3	9.5	92.9%	4.16 $\times 10^5$	73
I-NPF event at a coastal site of China	0.7	0.0135	98.2%	6.00 $\times 10^5$	16

Table 2. Major volatile organic compounds emitted by macroalgae as potential NPF precursors, sorted by TIC peak area measured by GC/MS or MS peak intensity measured by iodide-CIMS

	Formula	Structure	Peak area/MS peak intensity
1	C ₅ H ₁₂		1.90×10 ⁶
2	C ₅ H ₁₀		1.59×10 ⁶
3	CH ₃ I		1.37×10 ⁶
4	C ₃ H ₇ I		7.60×10 ⁵
5	CHBr ₃		4.71×10 ⁵
6	C ₅ H ₁₁ I		3.75×10 ⁵
7	CHBr ₂ Cl		2.71×10 ⁵
8	CH ₂ Cl ₂		2.55×10 ⁵
9	C ₁₀ H ₁₆		2.26×10 ⁵
1	C ₂ H ₆ O		1.70×10 ⁷
2	C ₃ H ₆ O		1.38×10 ⁷
3	C ₄ H ₆ O ₂		1.30×10 ⁷
4	C ₆ H ₁₂ O		1.03×10 ⁷
5	C ₅ H ₁₀ O		1.00×10 ⁷
6	C ₄ H ₁₀ O		5.16×10 ⁷
8	C ₂ H ₄ O		3.46×10 ⁷
9	C ₆ H ₁₀ O		2.88×10 ⁷
7	C ₅ H ₈ O		1.45×10 ⁷
10	C ₄ H ₈ O		1.37×10 ⁷
1	CH ₂ O ₂		1.58×10 ⁶
2	C ₂ H ₄ O ₂		9.52×10 ⁵
3	C ₃ H ₆ O ₃		9.21×10 ⁵
4	C ₆ H ₁₀ O ₃		4.44×10 ⁵
5	C ₂ H ₆ O ₂		2.88×10 ⁵
6	C ₄ H ₈ O ₂		1.17×10 ⁵

7

 $\text{C}_6\text{H}_{12}\text{O}_3$  1.12×10^5

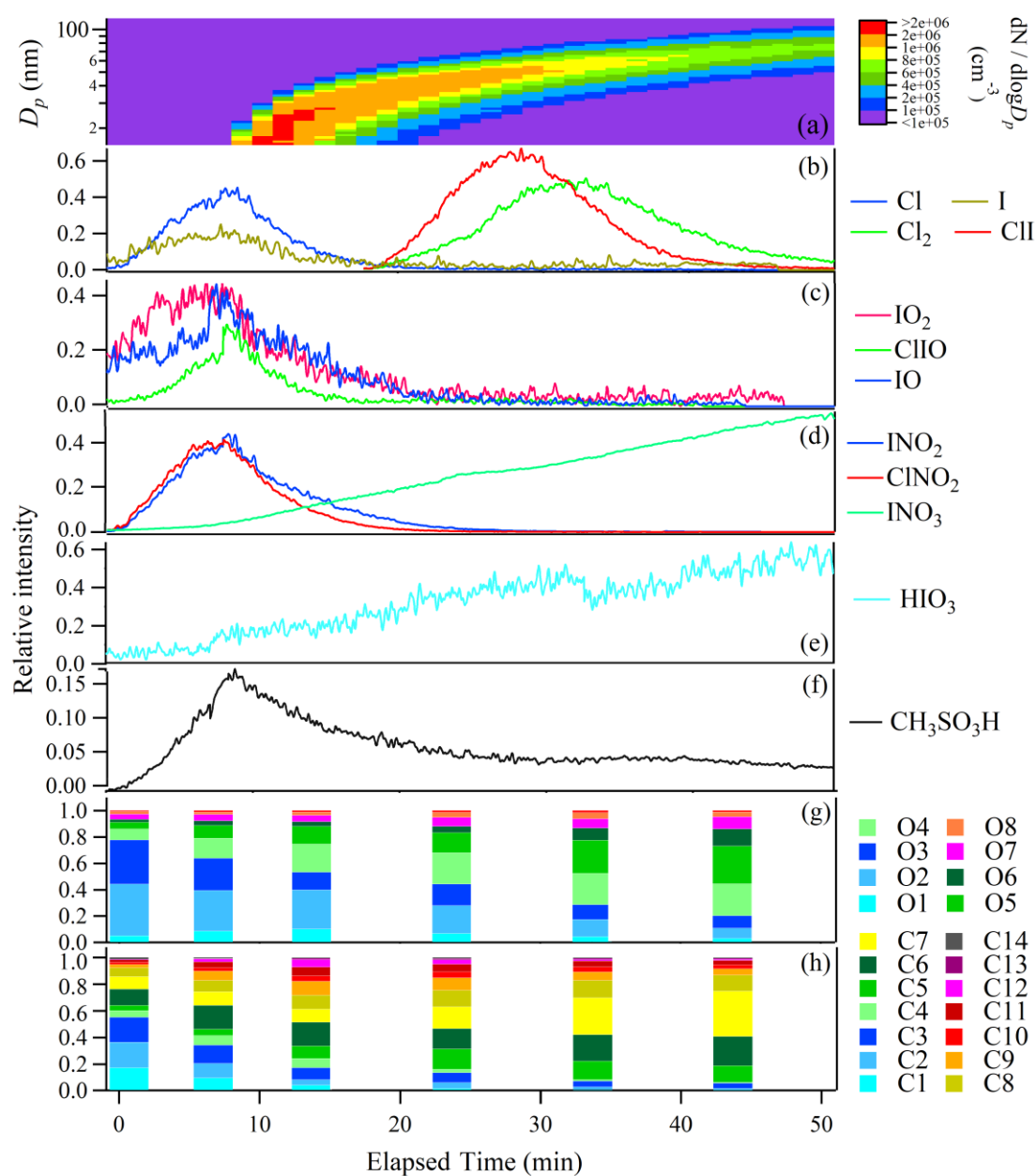


Figure 1. Time evolution of particle number size distribution (a) and relative intensities of gaseous molecules and radicals (b-f); the fractions of organic compounds grouped by O and C atom numbers in the selected time points (g-h) in a typical ozonolysis experiment (static mode). Time zero was chosen as the start time when HIO₃ was observed.

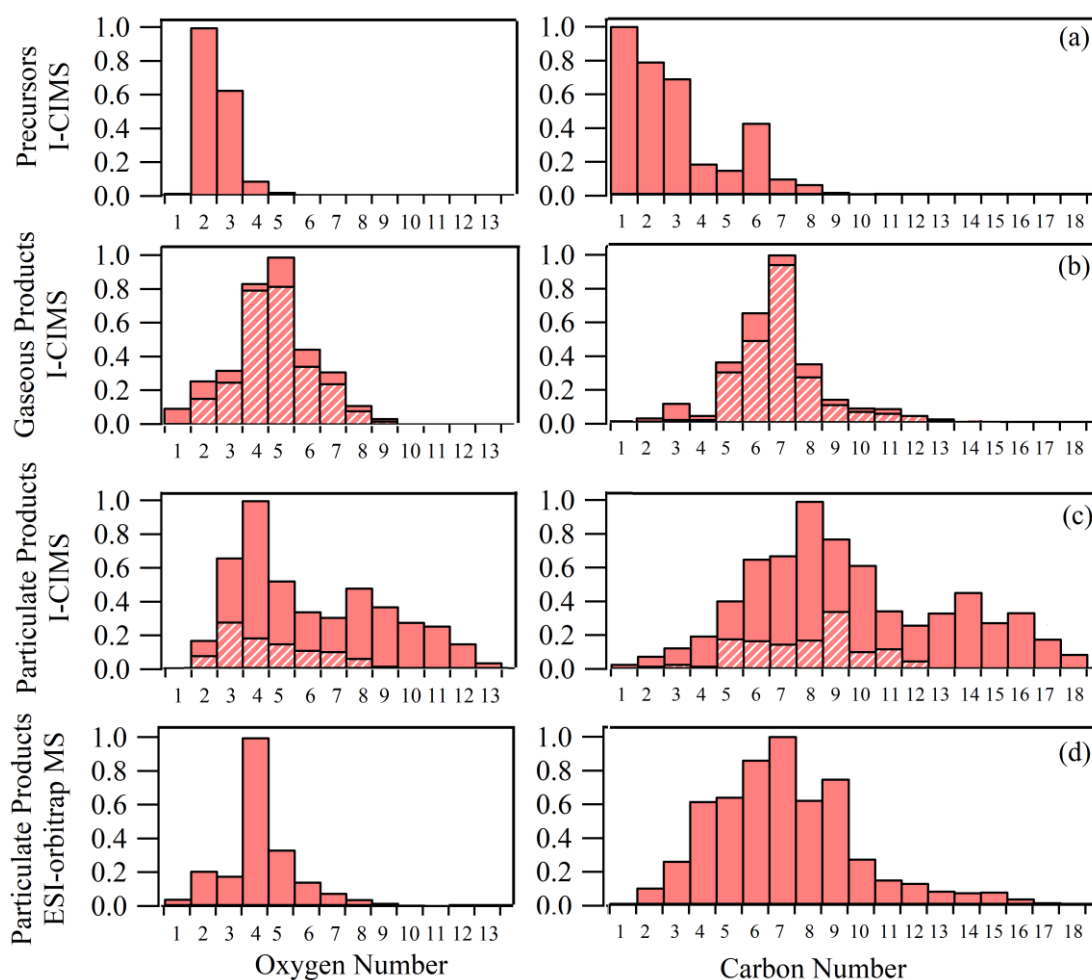


Figure 2. Oxygen and carbon atom number distributions of potential VOC precursors (a), gaseous products (b) and particulate products (c) measured by iodide-CIMS, as well as the particulate products measured by ESI-orbitrap MS (d) in a typical ozonolysis experiment (dynamic mode). Hatched bars indicate the fractions of organic formulas observed in both gas and particle phases by iodide-CIMS.